AGU PUBLICATIONS

Geophysical Research Letters

RESEARCH LETTER
10.1002/2016GL072373

Special Section:
The Arctic: An AGU Joint Special Collection

Air-sea gas transfer in high Arctic fjords

A. Andersson[1,2], E. Falck[3], A. Sjöblom[1,3], N. Kljun[4], E. Sahlée[1], A. M. Omar[5], and A. Rutgersson[1]

[1]Department of Earth Sciences, Uppsala University, Uppsala, Sweden, [2]Department of Ecotechnology and Sustainable Building Engineering, Mid Sweden University, Östersund, Sweden, [3]Department of Arctic Geophysics, University Centre in Svalbard, Longyearbyen, Norway, [4]Department of Geography, Swansea University, Swansea, UK, [5]Uni Research Climate, Bjerknes Centre for Climate Research, Bergen, Norway

Abstract In Arctic fjords and high-latitude seas, strong surface cooling dominates during a large part of the year, generating water-side convection (w_{*w}) and enhanced turbulence in the water. These regions are key areas for the global carbon cycle; thus, a correct description of their air-sea gas exchange is crucial. CO_2 data were measured via the eddy covariance technique in marine Arctic conditions and reveal that water-side convection has a major impact on the gas transfer velocity. This is observed even at wind speeds as high as 9 m s^{-1}, where convective motions are generally thought to be suppressed by wind-driven turbulence. The enhanced air-sea transfer of CO_2 caused by water-side convection nearly doubled the CO_2 uptake; after scaled to open-sea conditions the contribution from w_{*w} to the CO_2 flux remained as high as 34%. This phenomenon is expected to be highly important for the total carbon uptake in marine Arctic areas.

Key Points:
- From Arctic EC CO_2 data we show a dependence between water-side convection w_{*w} and the air-sea gas transfer velocity up to wind of 9 m s^{-1}
- The relative contribution from w_{*w} to the calculated total CO_2 flux was as high as 34%, where the magnitude is clearly related to u_{*w}/w_{*w}
- The convectively enhanced transfer results in a significantly larger oceanic CO_2 uptake by the sea in wintertime

Supporting Information:
- Supporting Information S1

Correspondence to:
A. Andersson,
andreas.andersson@geo.uu.se

Citation:
Andersson, A., E. Falck, A. Sjöblom, N. Kljun, E. Sahlée, A. M. Omar, and A. Rutgersson (2017), Air-sea gas transfer in high Arctic fjords, *Geophys. Res. Lett.*, *44*, 2519–2526, doi:10.1002/2016GL072373.

Received 23 DEC 2016
Accepted 26 JAN 2017
Accepted article online 28 JAN 2017
Published online 4 MAR 2017

1. Introduction

The absorption of atmospheric carbon dioxide (CO_2) by the world's oceans amounts to approximately 2.2 Pg C yr^{-1} [*Intergovernmental Panel on Climate Change*, 2013]. However, this uptake varies across all oceans and ocean sink/source behaviors might also shift depending on the season. The polar regions play an important role in the global marine system, acting as a major net sink of atmospheric CO_2 [*Takahashi et al*., 2002]. Air-sea exchange at these latitudes is also important for CO_2 cycling as carbon is transferred from the atmosphere to the ocean over long time scales and through deepwater formation. Polar waters are generally undersaturated with CO_2 and act as a sink for atmospheric CO_2 throughout the year. To understand the relationship between the carbon cycle and climate change, accurate models of the air-sea exchange of greenhouse gases at high latitudes are important.

Gas exchange across the air-water surface is controlled by the air-sea difference in the partial pressure of the specific gas and the gas transfer velocity. The gas transfer velocity describes the efficiency of the transfer process and is governed by various processes that cause turbulence in the subsurface water. Among these processes, wind speed is considered the most robust parameter for gas transfer velocity [e.g., *Liss and Merlivat*, 1986; *Wanninkhof et al*., 2009]. It is, however, generally agreed that the gas transfer velocity is controlled by a number of processes (e.g., surfactants, water-side convection, and rain), and a detailed understanding of the importance of these processes remains elusive [*Garbe et al*., 2014]. At higher wind speeds, wave breaking and encapsulated bubbles in the subsurface waters enhance the air-sea gas transfer velocity, and the magnitude of this enhancement likely depends on gas solubility [*Yang et al*., 2014; *Huebert et al*., 2010; *Marandino et al*., 2007; *Kihm and Körtzinger*, 2010; *Andersson et al*., 2016]. In contrast, in the low-wind speed regime, the transfer velocity may be governed by several parameters, such as rain, surfactants, microwave breaking, and water-side convection [*MacIntyre et al*., 2002; *Rutgersson et al*., 2011], depending on the regional conditions.

Few measurements of air-sea fluxes in high Arctic fjords have been reported [e.g., *Kilpeläinen and Sjöblom*, 2010; *Vihma et al*., 2011; *Kral et al*., 2014], and field studies on the parameters that affect the air-sea gas transfer velocity in polar areas are even scarcer. The surface conditions in these areas show great temporal complexity, involving, for example, ice formation, polynyas, currents, and convective mixing. Therefore, a more specific parameterization of the air-sea gas transfer velocity based on factors in addition to wind speed is necessary. Using the concept of resistances [*Liss*, 1973; *Jeffery et al*., 2007], *Rutgersson and Smedman* [2010] demonstrated that water-side convection was the main driver of water-side turbulence in situations with low wind speeds, unstable atmospheric stratification, and deepwater mixed layer depth. In wintertime, conditions of deepwater mixing and unstable stratification in the air and water commonly arise over the

North Atlantic and other high-latitude seas. In this study, we investigate the effect of water-side convection on the gas transfer velocity of CO_2 based on eddy covariance (EC) air-sea flux measurements of CO_2 and sensible and latent heat under Arctic marine conditions.

2. Theory

2.1. Transfer Velocity

Based on measurements of the air-sea flux of CO_2 (F_{CO_2}) and the difference in the partial pressure of CO_2 (ΔpCO_2) between surface water and overlaying air, the transfer velocity (k_{CO_2}) can be determined using the flux bulk equation:

$$k_{CO_2} = F_{CO_2}(K_0 \Delta pCO_2)^{-1} \tag{1}$$

where K_0 is the gas-specific solubility constant. To compare estimates of k_{CO_2} data measured at different locations with temperature T and salinity S, k_{CO_2} is normalized with respect to the Schmidt number (Sc).

$$k_{660} = k_{CO_2}(Sc/660)^{-1/2} \tag{2}$$

where k_{660} is the transfer velocity scaled to a Schmidt number of 660 (for CO_2 at 20°C in seawater). Numerous studies have investigated how to parameterize the transfer velocity in terms of horizontal wind speed at a height of 10 m (U_{10}; see the review by *Wanninkhof et al*. [2009]). A synthesized result from *Wanninkhof et al*. [2009] review is to use a parameterization that includes both quadratic and cubic wind speed terms, combining the effects from both low- and high-wind speed regimes:

$$k_{W09} = 3 + 0.1\ U_{10} + 0.064\ U_{10}^2 + 0.0011\ U_{10}^3 \tag{3}$$

Here the 10 m wind speed (m s^{-1}) is extrapolated from the wind speed measured at a height of 3 m above mean sea level, using the expression provided by *Högström* [1996] for the nondimensional wind gradient ϕ_m valid for unstable stratification; the measurement height was corrected for variations in the water surface level caused by the tide.

2.2. Water-Side Convection

Convective mixing is important for deepwater ventilation in the world's oceans. This mixing arises from surface buoyant forces generated by surface cooling and evaporation. As in the atmosphere, these large convective eddies are present throughout the mixed layer and are pronounced during low and moderate wind speeds. Close to the water surface, the convective eddies break down into smaller-scale water-side turbulence, which enhances the air-sea gas transfer. Similar to convective scaling in the atmosphere [*Deardorff*, 1970], an expression for the characteristic velocity scale (w_{*w}) of the convective turbulence in lakes [*Imberger*, 1985] and oceans [*Jeffery et al*., 2007] has been defined as

$$w_{*_w} = (Bz_{\mathrm{ml}})^{1/3} \tag{4}$$

where B is the buoyancy flux at the sea surface and z_{ml} denotes the mixed layer depth in water (the characteristic length scale). According to this expression, stronger buoyancy and deeper mixed layers produce enhanced water-side convection. To parameterize the buoyancy flux, an expression from *Jeffery et al*. [2007] is used.

$$B = \frac{gaQ_{\mathrm{net}}}{c_{\mathrm{pw}}\rho_w} + \frac{g\beta_{\mathrm{sal}}Q_E}{\lambda\rho_w} \tag{5}$$

The first term on the right-hand side describes the effect of surface cooling, where g is the gravity, a is the thermal expansion coefficient, and Q_{net} is the sum of the sensible and latent heat fluxes (Q_H and Q_E, respectively); the heat to or from the water body by advection; the net long-wave radiation (R_N); and the incoming short-wave radiation. c_{pw} denotes the specific heat of water at constant pressure, and ρ_w is the density of seawater. The second term describes the contribution of evaporation, where β_{sal} is the saline expansion coefficient and λ is the latent heat of vaporization. Here the incoming short-wave radiation is found to be in the range of 0–3 W m^{-2} (diffusive short-wave radiation), and vertical profile measurements of water temperature (not shown here) show no indication of horizontal differences in the water temperature. Based on EC flux

measurements performed in the Baltic Sea, *Rutgersson and Smedman* [2010] observed a significant enhancement of k with increasing surface cooling during unstable atmospheric stratification. After removing the impact of wind stress, they found that the gas transfer velocity (cm h^{-1}) increased as the convective turbulence increased in the range of 0.0062 m $s^{-1} < w_{*w} < 0.0166$ m s^{-1} according to the expression:

$$k_c = 3022 \ w_{*_w} - 20 \tag{6}$$

where a significant convective contribution was found when $w_{*w} > 0.01$ and $z_{ml} > 20$ m. At low to intermediate wind speeds, convection significantly enhances air-water gas transfer [*Eugster et al*., 2003; *Jonas et al*., 2003; *Rutgersson and Smedman*, 2010]. The general theory is that water-side convection is mainly important at lower wind speeds. In contrast, for higher wind speeds, stress-induced turbulence is typically dominant and disrupts the water-side convection, thereby reducing the influence of w_{*w} on k. Different suggestions have been proposed regarding when w_{*w} begins to be important for k. *MacIntyre et al*. [2002] found that water-side convection was the dominant process for air-water gas exchange when $U_{10} < 5$ m s^{-1}. Based on a lake study, *Imberger* [1985] proposed a relationship involving the ratio of the wind-driven water-side turbulence u_{*w} and w_{*w}, where water-side convection dominates when $u_{*w}/w_{*w} < 0.75$ with $u_{*_w} = u_* \left(\frac{\rho_a}{\rho_w}\right)^{1/2}$; here u_*denotes the friction velocity in air and ρ_a and ρ_w denote the densities of air and water, respectively. In contrast, *Podgrajsek et al*. [2014, 2015] determined that water-side convection was important for k_{CO_2} (and for the gas exchange of methane) for values of u_{*w}/w_{*w} exceeding 0.75 based on their study of a shallow lake. Data reflecting the importance of water-side convection for the gas transfer velocity at higher wind speeds, however, remain lacking.

3. Data and Analysis

3.1. Study Area and Measurements

A field campaign was conducted near Longyearbyen, Svalbard, Norway (Figure 1), between 14 and 30 March 2013. An EC flux tower and a tower containing profile instruments for temperature and wind were set up at Adventpynten, on the southwest side of Adventfjorden. Adventfjorden is a side fjord of the larger Isfjorden (north of Adventfjorden) and is approximately 7 km long. The distance across the fjord from Adventpynten is approximately 3 km. The fjord is surrounded by mountains rising to heights of 400–1100 m. The transition from land to water at the site is relatively smooth, but the water depth increases quickly. In the center of the bay, the bottom topography is relatively homogenous, and the water depth varies between 60 and 75 m. The EC flux method determines turbulent fluxes directly by correlating two high-frequency signals: the vertical wind component and the constituent of interest (e.g., CO_2). This method is frequently used for micrometeorological applications and has been applied to study several aspects of air-sea interaction in the study area [e.g., *Kilpeläinen and Sjöblom*, 2010; *Kral et al*., 2014]. The EC flux system was installed at 3 m above sea level (depending on the tide, which has a mean amplitude of roughly 1 m) and included one Sonic Anemometer CSAT3 (Campbell Scientific, North Logan, UT, USA) to measure the three wind components and sonic temperature and an LICOR-7500A (LICOR-Inc., Lincoln, NE, USA) open-path gas analyzer to measure humidity and CO_2. A second tower was also instrumented with slow-response sensors measuring wind, temperature, and humidity at 0.5 m and 4.0 m above the ground. On 14 and 19 March, profile measurements of water temperature and salinity were taken every 15 min near the tower in Adventfjorden at a water depth of approximately 45 m using a conductivity, temperature, and depth sensor (Sea-Bird SBE 19plus v2 SeaCAT, Sea-Bird Electronics Inc., Bellevue, WA, USA). Water samples were taken to determine the water concentration of dissolved inorganic carbon (DIC) and the alkalinity. In front of the boat, a net radiometer (CNR-1, Kipp & Zonen, Delft, Netherlands) was installed attached to a bar and used to measure the radiation balance over water. On 21 and 22 March, additional measurements of the radiation balance, pCO_2, and sea surface temperature (SST) were obtained using an SAMI 2 (Sunburst Sensors, Missoula, MO, USA) mounted at a depth of 0.5 m. The DIC was determined using a coulometric titration method with a precision of ~2 μmol kg^{-1}, and the alkalinity was obtained by potentiometric titration, which also had a precision of ~2 μmol kg^{-1}. The accuracy was measured by calibration against a certified reference material supplied by A. Dickson, Scripps Institution of Oceanography (U.S.). Then, the pCO_2 was calculated from the DIC, alkalinity, temperature, salinity, and pressure using CO2SYS software [*Lewis and Wallace*, 1998] and the dissociation constants of *Mehrbach et al*. [1973] refit by *Dickson and Millero* [1987].

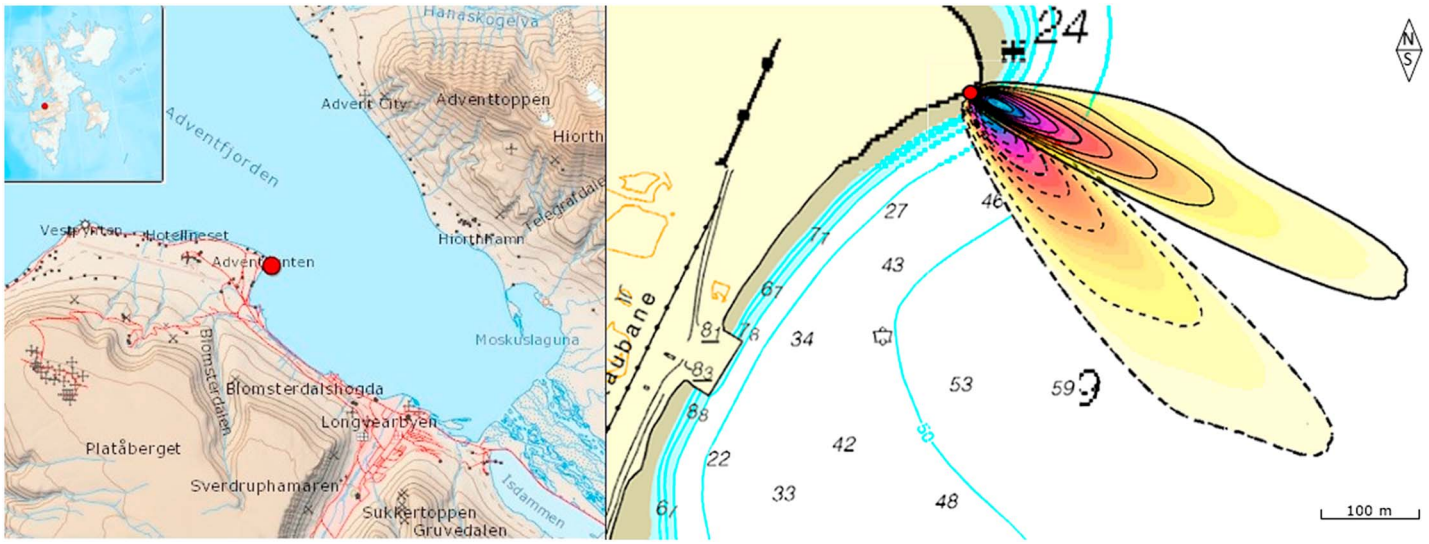

Figure 1. (left) Study area of Adventfjorden with the location of the site (red dot). The basemap was taken from TopoSvalbard (Norwegian Polar Institute, 2016). The inset in the left figure shows Svalbard and represents 73.9°N to 81.1°N and 8.9°E to 32.4°E. (right) The flux footprint contour lines are presented in 10% increments from 10% to 90% of the calculated total CO_2 flux footprint for Sector 1 (solid black line) and Sector 2 (dashed black line); the light blue lines are the isolines of the water depth.

3.2. Analysis

Flux data were sampled at a rate of 20 Hz and averaged over 30 min blocks. For every individual block, a double rotation and detrend algorithm was applied. Flux error caused by the time lag resulting from the distance separating the sonic and gas analyzers was reduced using an algorithm that finds the maximum correlation between the vertical wind and scalar (e.g., CO_2). Before the flux calculations, the data were screened with a filter using the diagnostic value of the LI-7500 and the mean concentrations of humidity and CO_2 to remove data affected by precipitation and ice growth on the instrument. The vertical turbulent fluxes were then determined based on the covariance of the turbulent element of the vertical wind and the turbulent part of CO_2. To account for the density fluctuations caused by heat fluxes affecting the measured CO_2 flux, the Webb-Pearman-Leuning correction [*Webb et al*., 1980] was applied. The EC method relies on the assumption of horizontal homogenous turbulence and stationary conditions, and thus, high-quality data are crucial. Fluxes measured at a certain height represent the surface conditions of a specific upwind area and comprise the flux footprint. For measurements collected at a land-based marine site, calculating the flux footprint is key for assessing the area of impact on the measurement. Here ensuring that the flux footprint corresponds to an area representative of the study area is important.

To investigate the size and location of the flux footprint and filter the data for further analysis, the flux footprint parameterization [*Kljun et al*., 2015] was run. Here the footprint climatologies for two cases were studied (Figure 1, right): one period with winds from the sector $90° < \text{wind direction (WD)} < 120°$ (Sector 1; black solid lines) and one period with winds from the sector $130° < \text{WD} < 150°$ (Sector 2; black dashed lines). The flux footprints were calculated for each 30 min flux measurement of the selected series and then aggregated to produce a footprint climatology for each case. For both sectors, most of the CO_2 fluxes originated from the 300 m range surrounding the EC tower. For Sector 1, the flux footprint is located over a region of the fjord with a water depth of 50–65 m and upwind fetch exceeding 3 km. For Sector 2 and situations in which WD >140, the upwind fetch is significantly reduced. Because of the possible risk of influence from the nearby harbor and the difference in wavefields for Sector 2 and Sector 1, only situations with wind from the sector $90° < \text{WD} < 130°$ were used for further analysis. The selected data were then evaluated by applying spectral and cospectral analyses, and data points associated with obvious errors were discarded.

4. Results

The air temperature varied between -16°C and -3°C during the field campaign, and wind speeds up to 14 m s^{-1} were measured. The wind direction was mostly in the range of $80° < \text{WD} < 150°$, resulting in the

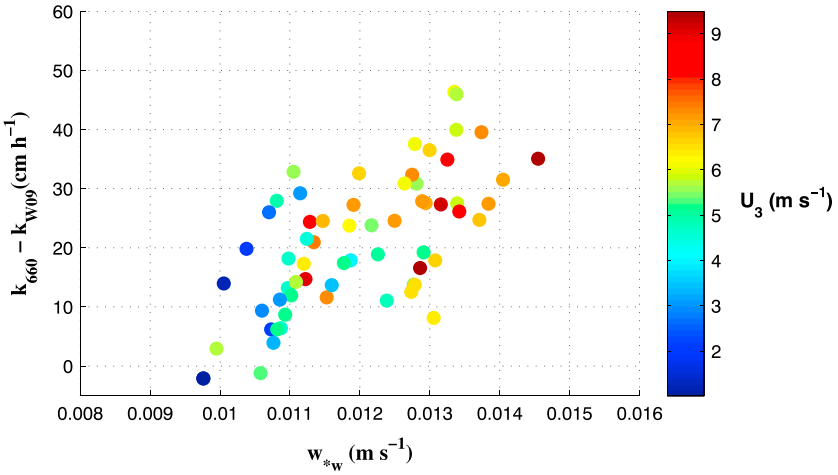

Figure 2. Plot of k_{660}–k_{W09} against the water-side convection velocity (w_{*w}); the colors denote the wind speed at a height of 3 m.

advection of dry, cold air from the land on the other side of the fjord over the comparatively warm open waters of Adventfjorden (water temperature: −1.0°C to −0.5°C). During the field campaign, three periods with wind from Sector 1 occurred. The first two periods (16–17 and 19–21 March) were characterized by winds from the sector 80°–150°, with limited icing of the instruments, and the EC CO_2 data were considered to be of good quality according to the spectral/cospectral analysis. During the last period (23–30 March), icing on the instruments was a major issue, and useful data were often reduced to a few hours immediately after the daily inspection of the instruments. The data characterizing the different periods are shown in Table S1 in the supporting information.

The incoming short-wave radiation was in the range of 0–3 W m^{-2} (diffusive short-wave radiation), and vertical profile measurements of water temperature (not shown here) showed no indications of horizontal differences in the water temperature. Hence, the calculation of Q_{net} was reduced to the sum of Q_H, Q_E, and R_N, where the outgoing long-wave radiation was in the range of 90–117 W m^{-2}. Both the sensible and latent heat fluxes showed maximum values exceeding 200 W m^{-2}, large but not uncommon for Arctic fjords in midwinter where heat fluxes exceeding 400 W m^{-2} are regularly observed [*Fortuniak et al.*, 2016]. The sensible heat flux was generally the larger of the two, with peak values close to 300 W m^{-2} associated with cold air outbreaks and $U_{10} > 10$ m s^{-1}. The average Bowen ratio B, which was defined as the ratio of sensible and latent heat fluxes, was 1.16. This value is similar to that measured by *Brümmer* [1997] ($B = 1.21$) in the same region during a cold air outbreak for upwind fetch in the range of 30–150 km.

Hydrographic measurements taken just outside Adventpynten showed a well-mixed water column all the way to the bottom (water depth of approximately 42 m). On 14 March, the SST was −0.50°C, and in the center of the fjord, the mixed layer depth was approximately 70 m. During 19–21 March, the surface water temperature varied between −0.56 and −0.53°C, and the salinity was close to 34.8 at all depths. Except for a period at the beginning of the field campaign, the CO_2 fluxes generally exhibited downward directions and were in the range of −5 to 0 μmol m^{-2} s^{-1}. These findings are in agreement with the measured pCO_2 in water of 250–278 μatm, suggesting CO_2 uptake by the water. Figure 2 depicts the convective contribution to the gas transfer velocity estimated from 62 half-hour measurements as a function of the convective velocity scale w_{*w}. The influence of wind speed-driven turbulence on the estimated gas transfer velocity was removed by k_{W09} (equation (3)). The color of each point corresponds to the wind speed measured at a height of 3 m above the mean sea level. The convective velocities are in the range of $0.0096 \text{ m s}^{-1} < w_{*w} < 0.0145 \text{ m s}^{-1}$ with wind speeds from 2.5 to 9.5 m s^{-1}. The largest contribution to w_{*w} comes from surface cooling (term 1 in equation (5)), whereas the contribution from changes in the salinity (term 2) is minor. A clear dependence is evident because k_{660}–k_{W09} increases as w_{*w} increases. For $0.010 \text{ m s}^{-1} < w_{*w} < 0.012 \text{ m s}^{-1}$, the convective velocities are generally associated with lower wind speeds. For situations with strong water-side convection ($w_{*w} > 0.010$ m s^{-1}) and relatively low wind speeds ($U_{10} < 6$ m s^{-1}), k_{660}–k_{W09} is expected to depend on w_{*w}. For higher wind speeds, however, the effect of water-side convection is generally assumed to be reduced by

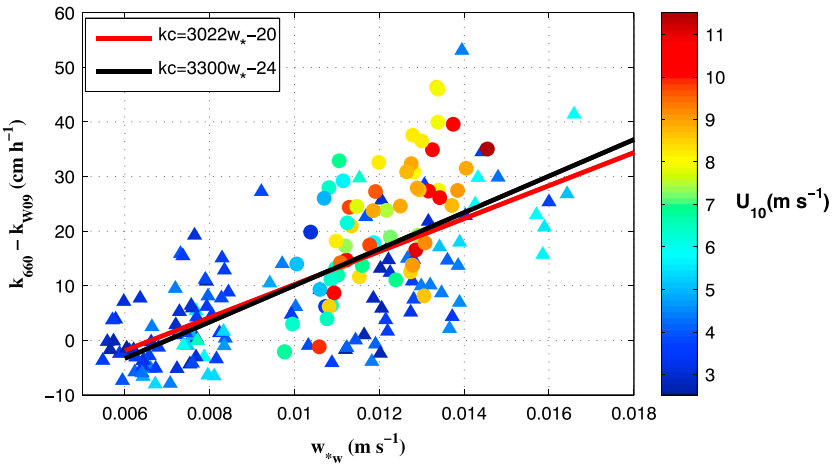

Figure 3. Plot of k_{660}–k_{W09} against the water-side convection velocity (w_{*w}) for Svalbard data (circles) and those of *Rutgersson and Smedman* [2010] (triangles). The colors of the symbols denote the wind speed at a height of 10 m (m s^{-1}). The black solid line shows the best linear fit to all data ($k_c = 3300\ w_{*w} - 24$) and describes the dependence between k_{660} andw_{*w}. The red line denotes the parameterization $k_c = 3022\ w_{*w} - 20$ of *Rutgersson and Smedman* [2010].

wind-driven turbulence. Here a regime with relatively high wind speeds (6–9.5 m s^{-1}) is found. Nevertheless, a significant contribution of water-side convection ($w_{*w} > 0.012$ m s^{-1}) was observed, with large values of k_{660}–k_{W09} and a dependence onw_{*w} that were similar to the low-wind-speed regime. Although these data are associated with high wind speeds, the large heat fluxes result in high values of w_{*w} and cause the ratio u_{*w}/w_{*w} to stay in the range of 0.9 to 1.4. The combination of wind-induced transfer and transfer caused by buoyant motions in the water under this regime results in the efficient air-sea transfer of CO_2. Indeed, the values of k_{660} are much larger than the calculated k_{W09} values that are normally used to estimate k_{660} at these high wind speeds.

Because of the limited fetch for these EC flux data, the wavefield within the flux footprint is not expected to exhibit the characteristics of a typical wavefield for open-sea conditions. Turbulence are generally higher over water bodies with limited fetch and growing sea conditions because, in the wavefield, the wave height is steeper and wavelength shorter than for open ocean with saturated waves. Studies on the turbulence characteristics over lakes have revealed that upwind surface roughness can affect the measured turbulence over a lake because of persistent larger eddies carry a memory of the upwind surface roughness over land [*Vesala et al.*, 2012]. The effect of the imbalance between u_* and U_3 on our results (i.e., the impact of the relationship between k_{660}–k_{W09} and w_{*w}) can be investigated by comparing the measured U_{10} with a wind speed representative of open-sea conditions. The latter can be calculated according to

$$U_{10,OS} = (u_*/\kappa)[\ln(z/z_{0C}) - \Psi_m] \tag{7}$$

where $\kappa$is the von Karman constant ($\kappa = 0.40$), and our measured values of u_*, the measurement height above sea level z, and the expression from *Charnock* [1955] for the roughness length $z_{0C} = \alpha \times u_*^2/g$ ($\alpha = 0.018$) are used. Ψ_m denotes the integrated profile function of wind speed, which is obtained from the integration of the expression for ϕ_m provided by *Högström* [1996]. Comparing the measured U_{10} and $U_{10,OS}$ showed that $U_{10,OS}$ was, on average, 30% higher than the measured U_{10}, and the largest differences between U_{10} and $U_{10,OS}$ were found at higher wind speeds. To validate and further investigate the contribution of k_{660} from water-side convection (k_c) and its dependence on w_{*w}, we use the data presented in *Rutgersson and Smedman* [2010] and *Rutgersson et al.* [2011], which were measured at the land-based marine site Östergarnsholm in the Baltic Sea [*Högström et al.*, 2008; *Rutgersson et al.*, 2008]. These data are associated with low wind speeds ($U_{10} < 6.5$ m s^{-1}) and cover water-side convective velocities in the range of 0.006 m s^{-1} $< w_{*w} <$ 0.018 m s^{-1}, with only a few values of $w_{*w} > 0.014$ m s^{-1}. As in Figure 2, which depicts the data from Adventfjorden, we use the wind speed parameterization of *Wanninkhof et al.* [2009], k_{W09}, to reduce the effect of wind-driven turbulence on k_{660} for the Östergarnsholm data (Figure 3). The two data sets show good agreement regarding the dependencies of k_c and w_{*w} (Figure 3), despite being measured under substantially different climatic conditions at different sites. The more moderate slope of the expression of

Rutgersson and Smedman [2010] for k_c given in equation (6) (cf. red line in Figure 3) causes a small underestimation of k_c for the Svalbard data. The best fit to both data sets is given by $k_c = 3300\ w_{*w} - 24$ (black line). When using $U_{10,OS}$ instead of U_{10} to remove the wind-driven turbulence, the best fit to the data is given by $k_c = 2300\ w_{*w} - 17$. For data associated with $U_{10,OS} < 7\ m\ s^{-1}$, however, the best fit to the data is $k_c = 2650\ w_{*w} - 19$. This is similar to the findings of *Rutgersson and Smedman* [2010], which were also based on data related to wind speeds $<7\ m\ s^{-1}$.

Finally, the relative importance of convectively generated turbulence for air-sea transfer is studied for an extended period using data for which k_c could be determined by measuring Q_H, Q_E, R_N, and z_{ml}, totaling 227 h of data from 16 to 31 March. Using the two parameterizations ($k_c = 3300\ w_{*w} - 24$ and $k_c = 2300\ w_{*w} - 17$), the relative CO_2 flux contributions to the total air-sea CO_2 flux from convectively driven flux F_c and wind-driven flux F_u (defined as $F_{tot} = F_u + F_c$ for simplicity) were estimated. The relative contribution of water-side convection to F_{tot} was found to depend on the ratio of u_{*w}/w_{*w}. On average, F_c accounted for 48% of F_{tot} using $k_c = 3300\ w_{*w} - 24$ and 34% of F_{tot} when $k_c = 2300\ w_{*w} - 17$ was used to determine F_c, and for $U_{10} < 7\ m\ s^{-1}$ the contributions to F_{tot} from F_c were calculated to 62% and 52%, respectively.

5. Summary and Conclusions

The importance of water-side convection for the efficiency of air-sea gas transfer was studied using EC measurements of CO_2 in an Arctic fjord region. The estimated transfer velocities of CO_2 show a clear dependence on the water-side convection generated by the surface cooling and evaporation of the water surface described by w_{*w}. For low wind speeds, previous studies have demonstrated that k_c (i.e., the contribution of water-side convection to the total transfer velocity for CO_2) can be expressed as a function of w_{*w}. Here we determined that this dependence is also valid for wind speeds as high as $9\ m\ s^{-1}$ for situations with strong water-side convection ($w_{*w} > 0.012\ m\ s^{-1}$). The combined effect of convectively driven turbulence and turbulence generated from wind forcing and breaking waves substantially improves the efficiency of gas transfer across the air-sea interface and results in significantly higher values of k_{660} relative to those obtained by a k_{660} parameterization based on wind speed alone. For comparison, we applied our approach to published data collected from Östergarnsholm in the Baltic Sea, which is exposed to very different climatic conditions. The two data sets showed good agreement in terms of the dependence of k_c on w_{*w}, which is best described by the parameterization $k_c = 3300\ w_{*w} - 24$. Based on our results, k_c affected the total gas transfer velocity to the same degree as the contribution of wind speed to the total gas transfer velocity. Our data, however, are associated with larger values of u_* than are typical for open-ocean conditions, partly because of the rougher water surface with steeper waves and shorter wavelengths, which led to increased surface roughness over the fjord.

When accounting for the potential underestimation resulting from wind stress on k_{660} compared to open-sea conditions, a dependence between k_{660}–k_{W09} and w_{*w} was found. The relative contribution of water-side convection to the calculated total CO_2 flux remained as high as 34%, and the magnitude is clearly related to u_{*w}/w_{*w}. Data associated with wind speeds lower than $7\ m\ s^{-1}$ show the strongest relationship between k_{660}–k_{W09} and w_{*w}, which is best described by $k_c = 2650\ w_{*w} - 19$, similar to the parameterization for k_c, as suggested by *Rutgersson and Smedman* [2010] for data with $U_{10} < 7\ m\ s^{-1}$.

This study demonstrates the importance of water-side convection for air-sea gas transfer. For Arctic fjords and coastal waters, water-side convection resulting from surface cooling likely significantly influences the total air-sea CO_2 exchange. Even if the conditions in the present study can be considered somewhat extreme, they are not uncommon for high-latitude seas in wintertime. Our results highlight that air-sea CO_2 transfer at these latitudes may be significantly underestimated, which has serious ramifications for estimates of the global carbon budget. Further investigations are urgently needed to improve our understanding of air-sea CO_2 exchange in marine Arctic areas.

Acknowledgments

The authors wish to thank Tor de Lange at the Geophysical Institute, University of Bergen, Norway, for his useful support and technical assistance during the fieldwork. We would like to extend special thanks to Werner Eugster and the two anonymous reviewers for their highly valuable feedback that improved the quality of this article. A.M. Omar is supported by the Centre for Climate Dynamics at the Bjerknes Centre. Data supporting the results will be provided upon request.

References

Andersson, A., A. Rutgersson, and E. Sahleé (2016), Using eddy covariance to measure air-sea gas transfer velocity for oxygen, *J. Mar. Syst.*, *159*, 67–75, doi:10.1016/j.jmarsys.2016.02.008.

Brümmer, B. (1997), Boundary layer mass, water, and heat budgets in wintertime, *Mon. Weather Rev.*, *125*, 1824–1837.

Charnock, H. (1955), Wind stress on a water surface, *Q. J. R. Meteorol. Soc.*, *81*(350), 639–640.

Deardorff, J. W. (1970), Convective velocity and temperature scales for the unstable planetary boundary layer and for Rayleigh convection, *J. Atmos. Sci.*, *27*, 1211–1213.
Dickson, A. G., and F. J. Millero (1987), A comparison of the equilibrium constants for the dissociation of carbonic acid in seawater media, *Deep Sea Res., Part A*, *34*, 1733–1743.
Eugster, W., G. Kling, T. Jonas, J. P. McFadden, A. Wüest, S. MacIntyre, and F. S. Chapin III (2003), CO_2 exchange between air and water in an Arctic Alaskan and midlatitude Swiss lake: Importance of convective mixing, *J. Geophys. Res.*, *108*(D12), 4362, doi:10.1029/2002JD002653.
Fortuniak, K., R. Przybylak, A. Araźny, W. Pawlak, and P. Wyszyński (2016), Sea water surface energy balance in the Arctic fjord (Hornsund, SW Spitsbergen) in May–November 2014, *Theor. Appl. Climatol.*, 1–12, doi:10.1007/s00704-016-1756-3.
Garbe, C. S., et al. (2014), Transfer across the air-sea interface, in *Ocean-Atmosphere Interactions of Gases and Particles*, edited by P. S. Liss and M. T. Johnson, pp. 55–112, Springer, Berlin Heidelberg.
Högström, U. (1996), Review of some basic characteristic of the atmospheric surface layer, *Boundary Layer Meteorol.*, *78*, 215–246.
Högström, U., et al. (2008), To what extent can we believe measurements on a land-based tower to represent upwind open sea conditions, *Boreal Environ. Res.*, *13*, 475–502.
Huebert, B. J., B. W. Blomquist, M. X. Yang, S. D. Archer, P. D. Nightingale, M. J. Yelland, J. Stephens, R. W. Pascal, and B. I. Moat (2010), Linearity of DMS transfer coefficient with both friction velocity and wind speed in the moderate wind speed range, *Geophys. Res. Lett.*, *37*, L01605, doi:10.1029/2009GL041203.
Imberger, J. (1985), The diurnal mixed layer, *Limnol. Oceanogr.*, *30*(4), 737–770, doi:10.4319/lo.1985.30.4.0737.
Intergovernmental Panel on Climate Change (2013), *The Physical Science Basis. Contribution of Working Group 1 to the Fifth Assessment Report of the Intergovernmental Panel on Climate Change*, edited by T. F. Stocker et al., pp. 1535, Cambridge Univ. Press, Cambridge, U. K., and New York.
Jeffery, C., D. Woolf, I. Robinson, and C. Donlon (2007), One-dimensional modelling of convective CO_2 exchange in the tropical Atlantic, *Ocean Modell.*, *19*(3-4), 161–182.
Jonas, T., A. Stips, W. Eugster, and A. Wüest (2003), Observations of a quasi shear-free convective boundary layer: Stratification and its implication on turbulence, *J. Geophys. Res.*, *108*(C10), 3328, doi:10.1029/2002JC001440.
Kihm, C., and A. Körtzinger (2010), Air-sea gas transfer velocity for oxygen derived from float data, *J. Geophys. Res.*, *115*, C12003, doi:10.1029/2009JC006077.
Kilpeläinen, T., and A. Sjöblom (2010), Momentum and sensible heat exchange in an ice-free Arctic fjord, *Boundary Layer Meteorol.*, *134*(1), 109–130.
Kljun, N., P. Calanca, M. W. Rotach, and H. P. Schmid (2015), A simple two-dimensional parameterisation for flux footprint prediction (FFP), *Geosci. Model Dev.*, *8*, 3695–3713, doi:10.5194/gmd-8-3695-2015.
Kral, S. T., A. Sjöblom, and T. Nygård (2014), Observations of summer turbulent fluxes in a high Arctic fjord, *Q. J. R. Meteorol. Soc.*, *140*, 666–675, doi:10.1002/qj.2167.
Lewis, E., and D. W. R. Wallace (1998), Program developed for CO_2 system calculations ORNL/CDIAC-105. Carbon Dioxide Information Analysis Center, Oak Ridge National Laboratory, Department of Energy, Oak Ridge, Tenn.
Liss, P. (1973), Processes of gas exchange across an air-water interface, *Deep Sea Res. Oceanogr. Abstr.*, *20*, *221–238*.
Liss, P., and L. Merlivat (1986), Air-sea gas exchange rates: Introduction and synthesis, in *The Role of Air-Sea Exchange in Geochemical Cycling*, edited by P. Buat-Menard, pp. 113–29, Reidel, Boston, Mass.
MacIntyre, S., W. Eugster, and G. W. Kling (2002), The critical importance of buoyancy flux for gas flux across the air-water interface, in *Gas Transfer at Water Surfaces*, *Geophys. Monogr.*, vol. 127, edited by M. A. Donelan et al., pp. 13–28, AGU, Washington, D. C.
Marandino, C. A., W. J. De Bruyn, S. D. Miller, and E. S. Saltzman (2007), Eddy correlation measurements of the air/sea flux of dimethylsulfide over the North Pacific Ocean, *J. Geophys. Res.*, *112*, D03301, doi:10.1029/2006JD007293.
Mehrbach, C., C. H. Culberson, J. E. Hawley, and R. M. Pytkowicz (1973), Measurements of the apparent dissociation constants of carbonic acid in seawater at atmospheric pressure, *Limnol. Oceanogr.*, *18*, 897–907.
Podgrajsek, E., E. Sahlée, and A. Rutgersson (2014), Diurnal cycle of lake methane flux, *J. Geophys. Res. Biogeosci.*, *119*, 236–248, doi:10.1002/2013JG002327.
Podgrajsek, E., E. Sahlée, and A. Rutgersson (2015), Diel cycle of lake-air CO_2 flux from a shallow lake and the impact of waterside convection on the transfer velocity, *J. Geophys. Res. Biogeosci.*, *120*, 29–38, doi:10.1002/2014JG002781.
Rutgersson, A., and A. Smedman (2010), Enhanced air–sea CO_2 transfer due to water-side convection, *J. Mar. Syst.*, *80*(1), 125–134.
Rutgersson, A., M. Norman, B. Schneider, H. Pettersson, and E. Sahlée (2008), The annual cycle of carbon dioxide and parameters influencing the air-sea carbon exchange in the Baltic Proper, *J. Mar. Syst.*, *74*, 381–394.
Rutgersson, A., A. Smedman, and E. Sahlée (2011), Oceanic convective mixing and the impact on air-sea gas transfer velocity, *Geophys. Res. Lett.*, *38*, L02602, doi:10.1029/2010GL045581.
Takahashi, T., S. C. Sutherland, C. Sweeney, A. Poisson, N. Metzl, B. Tilbrook, and J. Olafsson (2002), Global sea–air CO_2 flux based on climatological surface ocean pCO_2, and seasonal biological and temperature effects, *Deep Sea Res., Part II*, *49*(9), 1601–1622.
Vesala, T., W. Eugster, and A. Ojala (2012), Eddy covariance measurements over lakes, in *Eddy Covariance: A Practical Guide to Measurement and Data Analysis*, edited by M. Aubinet, T. Vesala, and D. Papale, pp. 365–376, Springer, Netherlands.
Vihma, T., T. Kilpeläinen, M. Manninen, A. Sjöblom, E. Jakobson, T. Palo, J. Jaagus, and M. Maturilli (2011), Characteristics of temperature and humidity inversions and low-level jets over Svalbard fjords in spring, *Adv. Meteorol.*, *2011*, 486807, doi:10.1155/2011/486807.
Wanninkhof, R., W. E. Asher, D. T. Ho, C. Sweeney, and W. R. McGillis (2009), Advances in quantifying air-sea gas exchange and environmental forcing, *Annu. Rev. Mar. Sci.*, *1*, 213–44.
Webb, E. K., G. I. Pearman, and R. Leuning (1980), Correction of flux measurements for density effects due to heat water vapor transport, *Q. J. R. Meteorol. Soc.*, *106*, 85–100.
Yang, M., B. Blomqvist, and P. Nightingale (2014), Air-sea exchange of methanol and acetone during HiWinGS: Estimation of air phase, water phase gas transfer velocities, *J. Geophys. Res. Oceans*, *119*, 7308–7323, doi:10.1002/2014JC010227.